PAPER

Check for updates

Towards the best total consumption infrared-heated sample introduction system for nanoparticle measurement using single particle inductively coupled plasma mass spectrometry†

Zichao Zhou,[a] Mirah J. Burgener,[b] John Burgener[c] and Diane Beauchemin [ID] *[a]

Nanoparticles (NPs) are ubiquitous because they find applications in nanomedicine, materials science, and consumer products to name a few, and eventually end up in the environment. The various techniques available to analyze NPs each have strengths and limitations. This study focuses on improving the single particle inductively coupled plasma mass spectrometry (spICPMS) technique to address the limitations of existing methods and improve the size detection limit for Pt and Au NPs. Infrared heating of the spray chamber and connection to the torch is used to pre-evaporate the aerosol and improve the transport efficiency. Eight modified cyclonic spray chambers with a volume ranging from 25 to 125 mL, where an IR emitter is inserted in a modified baffle and the gap between the top of the baffle and the top service of the spray chamber was varied, are tested for the characterization of NPs to see their effect on sensitivity, detection limit, and transport efficiency. The results indicate that the 50 mL modified spray chamber with a 2 mm gap between the top of the baffle and the top service of the spray chamber offers the best detection limit for Pt. It enhances sensitivity and precision and allows accurate characterization of Au and Pt NPs without any measurement of the transport efficiency. Furthermore, this sample introduction system provided similar improvements in sensitivity and detection limit when used with the same nebulizer on two different spICPMS instruments.

Introduction

Nanoparticles (NPs), which measure less than 100 nm in size,[1] have become ubiquitous because they possess unique properties that make them important in various industries. For instance, they find applications in nanomedicine, materials science, and consumer products to name a few. Because they eventually end up in the environment,[2–5] risk assessment requires knowledge of NPs characteristics, including size, composition, number concentration, and surface properties.

To characterize NPs, several techniques can be used, including dynamic light scattering, transmission electron microscopy (TEM) and atomic force microscopy.[6–8] However, they are not without limitations.[9] Many of them are primarily ensemble methods, averaging the characteristics of a large population of NPs. Some of them have inadequate sensitivity when applied to environmental systems.[10,11] Additionally, they

[a]*Department of Chemistry, Queen's University, Kingston, ON K7L 3N6, Canada. E-mail: diane.beauchemin@queensu.ca; Fax: +1-613-533-6669; Tel: +1-613-533-2619*
[b]*Burgener Research Inc., 9710 Second Street, Unit #103, Sidney, BC V8L 3C4, Canada*
[c]*Burgener Research Inc., 1680 Lakeshore Road West, Unit #2, Mississauga, ON L5J 1J5, Canada*

† Presented in part at the 2024 Winter Conference on Plasma Spectrochemistry, Tucson, AZ, USA.

often require sample preparation steps that can introduce contamination and potentially alter NPs. For example, ferromagnetic Ni NPs have been noted to spontaneously agglomerate in the vacuum environment of TEM.[12] In contrast, inductively coupled plasma mass spectrometry (ICPMS) in single particle mode (called spICPMS) readily allows the sensitive and element-specific measurement of NPs individually in solution.

In fact, spICPMS can measure the mass (and the size if characteristics like density, shape, and composition are known) and quantify the concentration of suspended NPs, in addition to simultaneously determining the concentration of dissolved analytes.[13,14] Its application to a variety of samples has been the subject of a comprehensive review.[15] The detection of the smallest NPs highly depends on the sensitivity and detection limit (DL) of ICPMS. Consequently, techniques employed to enhance the DL in solution analysis *via* ICPMS may also be useful for spICPMS.[16] Indeed, experimental conditions have a substantial impact on the resulting NPs signals,[17] especially the sample introduction system,[18] which must be carefully designed and optimized to ensure the reliability, efficiency, and accuracy of the measurements.

However, a NPs suspension is usually introduced with a conventional pneumatic sample introduction system in spICPMS, where only 5–10% of the nebulized aerosol reaches

the plasma, the rest draining down to waste.[19] Such low transport efficiency limits sensitivity and DL. As a result, the transport efficiency must be measured in addition to the sample uptake rate in spICPMS to enable accurate measurement of NPs mass, size and concentration. However, transport efficiency is difficult to determine in the absence of certified reference NPs matching those in samples. Coupling flow injection[12] or monosegmented flow analysis[20] to spICPMS eliminates the requirements to determine the transport efficiency and the sample uptake rate for measurement of the mass, and thus size, of NPs. Similarly, integrating the signal instead of averaging it in spICPMS[21] eliminates the need to measure the transport efficiency when determining NPs mass and size. However, determination of NPs concentration still requires measurement of the transport efficiency. The requirement to measure the transport efficiency for determination of NPs concentration would vanish with an approach providing 100% transport efficiency.

The heated torch-integrated sample introduction system (hTISIS) has successfully achieved total sample consumption and enhanced sensitivity in ICPMS,[22] but the micro-nebulizer used with the hTISIS is susceptible to blockage when dealing with samples containing high salt concentrations. A micro-droplet generator, employed in spICPMS also provides 100% transport efficiency,[23] but it generates a dry aerosol, which adversely affects plasma ionization by removing water.[24] To enhance transport efficiency while mitigating noise attributed to droplet desolvation in the plasma, an alternative approach involves infrared (IR) heating to pre-evaporate the aerosol before its introduction into the plasma.[25,26] In spICPMS, a 50 mL cyclonic spray chamber was modified to enable the insertion of an IR emitter within a modified baffle, with a 2 mm gap between the top of the baffle and the top service of the spray chamber; at 50 µL min^{-1} sample uptake rate and 110 °C IR heating temperature, essentially total consumption was achieved, which translated into 5-fold improvements in sensitivity and solution DL.[26] However, difficulty with heating the torch base located within the torch box increased the noise level, resulting in only a 2-fold improvement in size DL.

Building upon prior research, the aim of this study was to perform a comprehensive optimization of an IR-heated sample introduction system. To this end, eight modified cyclonic spray chambers, with varying volumes and dimensions, were compared with the objective to improve the size DL for Pt and Au. The most efficient configuration was subsequently employed for the analysis of certified suspensions of Au and Pt NPs using two different ICPMS instruments, including one where the base of the torch could be directly heated.

Experimental

Instrumentation. Optimization of the sample introduction system was conducted using a Varian 820MS quadrupole-based ICPMS instrument (Varian Inc., Australia) equipped with Ni sampler and skimmer cones with orifice diameters of 0.9 mm and 0.4 mm, respectively. A PFA 260 nebulizer (Burgener Research Inc., Mississauga, ON, Canada) was used with all spray chambers. The sample uptake rate was controlled by a Rainin Rabbit Plus peristaltic pump (Rainin, Mack Road, Woburn, MA, USA). The IR-heated sample introduction system featured a modified baffled cyclonic spray chamber (MC) with a shortened neck and an "L" shaped elbow connection (JRV Scientific Glass, Montreal, QC, Canada). Ball joints of glass parts were held together by metal clips. Four different volumes of MCs were tested: 25, 50, 75 and 125 mL. A 2 mm gap between the top of the modified baffle and the top service of the spray chamber (denoted 50-2 mm for a 50 mL MC with 2 mm gap in Fig. 1) ensured that only the finest droplets, alongside those in a gaseous state, could egress from the spray chamber. Two additional 50 mL and 75 mL MCs were fabricated with two other gaps: 4 and 6 mm.

To heat each of the 8 chambers, a ceramic rod IR heater with an integrated thermocouple (Elstein-Werk, Northeim, Germany) was inserted into the modified baffle. To prevent condensation between the spray chamber and the base of the torch, a ceramic beaded rope IR heater (Marsh Beaded Heaters, Normangee, TX, USA) was wrapped around the sheathing device and elbow connection. Temperature control was achieved by the thermocouple with pen heater and a thermocouple inserted under the IR rope heater, which were regulated using two identical Digi Toll II temperature controllers (GLAS-COL Apparatus Company, Terre Haute, USA). The entire system was enveloped with glass-fiber heat insulating tape and aluminum foil to ensure consistent heating and minimize heat loss. For reference, a Scott double-pass spray chamber (SCP Science, Baie d'Urfé, QC, Canada) was employed.

To evaluate the performance of the total consumption sample introduction system for spICPMS in time-resolve mode, a NexION 2000 ICPMS instrument (PerkinElmer, Waltham, Massachusetts, United States) was also used. In contrast to the Varian 820MS instrument, the torch base is outside the torch box and can be heated to prevent condensation. The L-shaped elbow was thus directly connected to the base of the torch (without any sheathing device). A custom-made ball joint torch connector was made from an open-end male ball joint and a Teflon sleeve. The operating conditions are summarized in Table 1. The standard sample introduction system used on the NexION 2000 instrument for reference consisted of a PFA 260 nebulizer and a glass cyclonic C3 high sensitivity spray chamber with matrix gas port. The nebulizer gas flow rate in Table 1
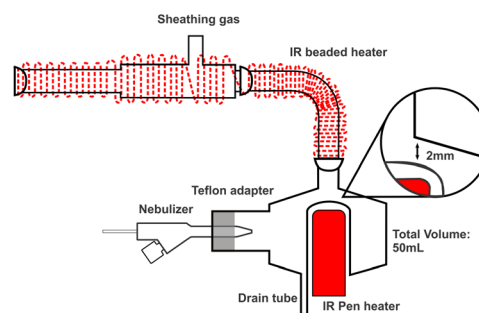

Fig. 1 Schematic diagram of the IR-heated sample introduction system with a "50-2 mm" modified cyclonic spray chamber.

This journal is © The Royal Society of Chemistry 2024

J. Anal. At. Spectrom., 2024, **39**, 2078–2086 | **2079**

Table 1 spICPMS operating parameters

Parameter	Varian 820MS	NexION 2000
Ar plasma gas flow rate (L min^{-1})	18.0	15.0
Ar auxiliary gas flow rate (L min^{-1})	1.80	1.20
Ar sheath gas flow rate (L min^{-1})	0.20	—
Ar nebulizer gas flow rate (L min^{-1})	0.90	1.00
RF power (kW)	1.30	1.60
Dwell time (ms)	5	0.05
Monitored signal	$^{195}Pt^+$ or $^{197}Au^+$	

resulted from optimization using the standard sample introduction system on each instrument.

Materials. Multielement standard solutions (0.1–10 µg L^{-1}) were prepared in 2% v/v HNO$_3$ from 1000 mg L^{-1} Au and 10 000 mg L^{-1} Pt standard solutions (SCP Science, Baie d'Urfé, QC, Canada), sub-boiled HNO$_3$ and doubly deionized water (DDW) (18.2 MΩ cm). A 5 ng mL^{-1} multielement tunning solution was prepared from ICPMS stock tunning solution, sub-boiled HNO$_3$ and DDW. A DST-1000 sub-boiling distillation system (Savillex, Minnetonka, MN, USA) was used to purify HNO$_3$ (ACS grade; Fisher Scientific, Ottawa, ON, Canada). For validation, two suspensions of reference NPs were used: Au NPs in water (99.99% purity; diameter of 60.6 ± 5.9 nm) with a concentration of 50 mg mL^{-1} and bare Pt NPs in water (99.99% purity; diameter of 50 ± 4 nm) purchased from nanoComposix (San Diego, CA, USA). These NPs were stabilized in citrate buffer and have a near spherical geometry. Certified NP suspensions were diluted to 100 000 particles mL^{-1} with DDW to ensure that each droplet produced during nebulization would contain at the most one NP. To avoid NP dissolution and aggregation, dilution was performed on the day of the analysis followed by sonication for 10 min prior to analysis.

Optimization. A 5 µg L^{-1} multielement standard solution and its corresponding blank were analyzed in peak hopping mode using the Bruker Quantum software to quickly determine sensitivity. Minitab Release 17 statistical software (Minitab Inc., State College, PA, USA) and a face-centered composite experimental design were used to study the effect of the IR heating temperature and sample uptake rate for each IR-heated MC, with the aim to find the conditions providing the best compromise in terms of sensitivity, plasma robustness (as indicated by $^9Be^+/^7Li^+$),[27] doubly-charged ion and oxide ratios. Based on the previous study, where the optimum temperature was 100 °C after optimizing it over the 20–300 °C range,[26] a multivariate optimization was conducted over a narrower temperature range (20–200 °C) while the sample uptake rate was varied from 25 to 75 µL min^{-1}. After installation of the optimized IR-heated sample introduction system on the NexION 2000 instrument, the nebulizer gas flow rate was optimized over the range of 0.9 to 1.2 L min^{-1}, in increments of 0.02 L min^{-1}.

Measurement of sample uptake rate and transport efficiency. The sample uptake rate was measured in triplicate by weighing a vial containing DDW before and after 5 min of aspiration. Five replicate measurements of the transport efficiency were made while nebulizing a suspension of NPs, as the fraction of NPs detected over those nebulized.[17]

Data processing. An external calibration using standard solutions, which correlated signal intensity with analyte concentration, was converted into a calibration relating signal intensity to mass per event by multiplying the analyte concentration by the sample uptake rate, transport efficiency, and dwell time. NP events were identified through an iterative process as any signal exceeding the average intensity value of the dataset by more than three times the standard deviation.[17] Because this is automatically done by the Syngistix software of the NexION 2000 instrument, which uses Gaussian statistics to determine the particle detection threshold, Gaussian statistics were also used to manually process data from the Varian 820MS instrument to enable direct comparison. The average signal left after NP selection served as the blank for determination of the method DL. The full equation of the calibration was then used to convert each blank-subtracted NP signal to a mass, which was finally converted to a size using the density of the metal and using a spherical geometry. A size distribution was generated by binning NPs of similar size together.

Measurement of the transport efficiency required a correction for the significant settling time of the Varian 820MS instrument,[21] which necessitated approximately 27 ms on average for data transfer following each dwell time, even when monitoring a single mass-to-charge ratio. To account for this time during which no NP could be measured, the calculated transport efficiency was adjusted by multiplying it by the fraction of the total acquisition time during which actual measurements were taken (*i.e.* by 5/(5 + 27)). The method size DL was determined using a suspension of NPs, based on three times the standard deviation of the background signals left after removing the signals generated by NPs.

Results

Optimization. Two optimizations were carried out for each spray chamber. For the first, the sample uptake rate ranged from 25 to 75 µL min^{-1} while the IR heating temperature ranged from 20 to 200 °C and the focus was on maximizing sensitivity. Analysis of contour plots of the resulting blank-subtracted signal intensity of a 5 ng L^{-1} Au standard solution (of which a representative example is shown in Fig. 2a) revealed that optimal sensitivity resulted with 60–150 °C IR heating temperature and 40–60 µL min^{-1} sample uptake rate for the 25-2 mm MC.

In a second optimization aiming to find the best compromise in terms of plasma robustness, doubly charged ion ratio, oxide ratio, and transport efficiency, the IR heating temperature was increased in 10 °C increments from 60 to 150 °C, with the sample uptake rate held constant at 50 µL min^{-1} (Fig. 2b). The $^9Be^+/^7Li^+$ ratio was reported to be comparable to the Mg II 280.270 nm/Mg I 285.213 nm ratio in ICP optical emission spectrometry because Be and Li have similar atomic masses but different first ionization potentials so that the $^9Be^+/^7Li^+$ ratio is sensitive to plasma conditions while not being strongly affected by space charge effects occurring in the ion optics of the mass spectrometer.[27] Robust plasma conditions, with a $^9Be^+/^7Li^+$ ratio of at least 0.30, were achieved over the range of IR heating

2080 | *J. Anal. At. Spectrom.*, 2024, **39**, 2078–2086
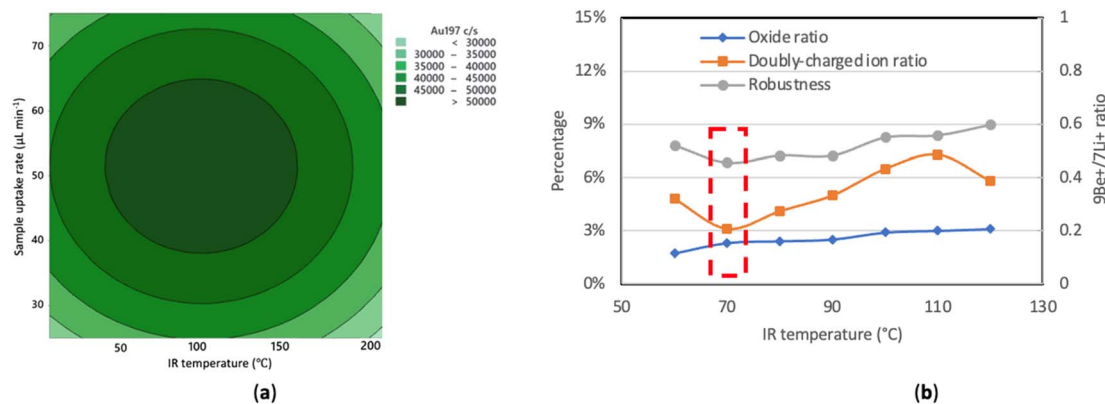
This journal is © The Royal Society of Chemistry 2024

Fig. 2 Results of optimizations for 25-2 mm MC (a) Contour plot of blank-subtracted signal intensity for 5 μg L^{-1} Au vs. sample uptake rate and IR heating temperature; (b) oxide ratio, doubly charged ion ratio and robustness (Be$^+$/Li$^+$ signal ratio)[27] at different IR heating temperatures while other parameters were held constant. The optimum temperature is indicated by the dashed red box.

temperatures tested with the 25-2 mm MC. In this example, 70 °C maximized sensitivity and robustness while keeping the oxide and doubly-charged ion levels around and under 3%, respectively, but did not quite result in total consumption with the Varian 820MS. The apparent discrepancy stems from sensitivity being measured with solutions whereas the transport efficiency was measured with a suspension of NPs. Given that total consumption was achieved with the 25-2 mm MC IR-heated at 70 °C when it was directly connected to the base of the torch on the NexION instrument (see Table 5), NPs likely deposited through aerosol condensation in the unheated region between the sheathing device and the torch inside the torch box of the Varian 820MS instrument.

Effect of spray chamber volume. Four modified cyclonic spray chambers having different sizes (25, 50, 75 and 125 mL) but the same 2 mm gap between the top of the modified baffle and the top service of the spray chamber were tested. Table 2 shows that all four of the IR-heated MC spray chambers resulted in a significant improvement in transport efficiency compared to that achieved with the Scott double-pass spray chamber at room temperature when using the same nebulizer at the optimal sample uptake rate. This is not solely a result of the spray chamber design, as Table 3 shows that total consumption was not achieved

with any of the spray chambers without IR heating using the same nebulizer at the same sample uptake rate. Total consumption was achieved upon IR heating with the 50 mL and 75 mL MCs. With the four MCs, improvements in sensitivity ranged from 3 to 10 times. However, the DL did not improve as much.

Compared to the unheated double-pass spray chamber, the 75-2 mm MC increased sensitivity but did not significantly improve the solution and method DLs, whereas the 125-2 mm MC improved the sensitivity and degraded DLs. As the volume of the spray chamber increased, the optimal IR heating temperature also increased under the otherwise constant operating conditions in Table 1. The size of the IR heater being constant, there might be a temperature gradient between the center of the baffle and the outer shell of the spray chamber without increasing the temperature. This was verified using thermocouples placed in the baffle and on the outer surface of the spray chamber. For example, when the inner baffle of the 50-2 mm MC (with the operating conditions in Table 1 and a sample uptake rate of 50 μL min^{-1}) was heated to 110 °C, the outer surface was 88 °C. Such temperature gradient increased as the spray chamber volume increased.

Another difference between the spray chambers is that the distance between the nebulizer tip and the central baffle

Table 2 Figures of merit for spICPMS with 5 different volume spray chambers under optimum conditions on Varian 820MS

Spray chamber	Double-pass	25-2 mm MC	50-2 mm MC	75-2 mm MC	125-2 mm MC
IR temperature (°C)	20	70	110	120	150
Sample uptake rate (μL min^{-1})	1000	50.0 ± 5.0	50.0 ± 5.0	50.0 ± 5.0	50.0 ± 5.0
Transport efficiency (%)	8.1 ± 3.4	86.3 ± 6.4	102.2 ± 5.4	98.2 ± 7.4	65.2 ± 6.4
^{195}Pt sensitivity (counts s^{-1} μg^{-1})	2.66 × 10^{10}	2.72 × 10^{11}	1.56 × 10^{11}	1.16 × 10^{11}	1.03 × 10^{11}
^{197}Au sensitivity (counts s^{-1} μg^{-1})	3.23 × 10^{10}	4.27 × 10^{11}	2.27 × 10^{11}	1.24 × 10^{11}	1.36 × 10^{11}
^{195}Pt solution DL (ng L^{-1})	12	3.6	1.7	8.1	18
^{197}Au solution DL (ng L^{-1})	11	2.3	2.6	7.9	14
^{195}Pt method size DL (nm)	22	11	5.9	14	39
^{197}Au method size DL (nm)	22	7.6	8.6	16	29
^{9}Be$^+$/^{7}Li$^+$	0.28	0.46	0.33	0.22	0.24
^{140}Ce^{16}O$^+$/^{140}Ce$^+$	1.5%	3.1%	4.8%	1.4%	2.5%
^{138}Ba^{++}/^{138}Ba$^+$	0.5%	2.3%	0.7%	3.3%	3.4%

Table 3 Transport efficiency (mean ± standard deviation, $n = 5$) at room temperature (20 °C) and 50 μL min^{-1} sample uptake rate with different spray chambers

Spray chamber	Transport efficiency (%)	Spray chamber	Transport efficiency (%)
Scott double-pass	14.7 ± 1.7	75–2 MC	10.1 ± 1.9
25–2 MC	26.0 ± 5.6	75–4 MC	11.4 ± 2.1
50–2 MC	24.9 ± 2.6	75–6 MC	10.0 ± 2.8
50–4 MC	20.1 ± 3.5	125–2 MC	4.6 ± 3.1
50–6 MC	23.5 ± 3.1		

increased as the spray chamber volume increased, from 1.3 cm with the 25-2 mm MC to 3.8 cm with the 125-2 mm MC. This likely affected the droplet size distribution of the secondary aerosol that experiences IR heating, in turn affecting the extent of pre-evaporation. A temperature gradient combined to sub-optimal positioning of the nebulizer may thus explain differences in sensitivity and transport efficiency between spray chambers, such as why the 125 mL MC yielded a lower sensitivity and transport efficiency than the 50 mL and 75 mL ones. Future work will investigate the effect of IR heating the top of the spray chamber in addition to having an IR emitter within the baffle. As well, the design of each spray chamber will be modified to allow optimal positioning of the nebulizer.

The results in Table 2 were obtained under plasma conditions optimized using the standard sample introduction system with the same nebulizer. However, a preliminary multivariate optimization of the sheath gas flow rate and of the nebulizer gas flow rate with the 50-2 mm MC IR-heated at 110 °C and a sample uptake rate of 50 μL min^{-1} (Fig. 3) revealed that higher sensitivity would result using a nebulizer gas flow rate of 0.8–0.85 L min^{-1} (instead of the 0.9 L min^{-1} used in this work) and a sheath gas flow rate of 0.07–0.08 L min^{-1} (which is substantially lower than the 0.2 L min^{-1} used in this work). Further improvements in sensitivity and detection limit are thus likely under thoroughly optimized conditions. Hence, future work will also include multivariate optimization of the nebulizer gas flow rate, sheathing gas flow rate, sampling position and IR temperature with each spray chamber to achieve the best possible balance between sensitivity, detection limits, and plasma robustness.

In any case, even under plasma conditions optimized with the standard sample introduction system, the 25-2 mm MC, 50-2 mm MC and 75-2 mm MC improved the solution and method size DLs compared to those obtained with a double-pass spray chamber. With the 50-2 mm MC, the lowest size DL resulted for Pt, with similar size DL as with the 25-2 mm MC for Au. The 50-2 mm MC thus provides total consumption while improving sensitivity and DLs. Compared to the results previously obtained with the 50-2 mm MC also IR-heated to 110 °C and operated at a sample uptake rate of 50 μL min^{-1},[26] a greater improvement in size DLs was achieved in this work because of the insulating tape that was wrapped around the elbow connection under the aluminum foil. (Only aluminum foil was employed in the previous study.) The 50-2 mm MC also leads to robust conditions and low doubly-charged ion level, with a concurrent increase in oxide level however. This is surprising, as robust conditions typically correspond to a hotter plasma, which normally translates into lower oxide level and increased doubly-charged ion level. Investigation of this apparent discrepancy will be the subject of future work. Nonetheless, as the 3–4 fold improvement in size DL does not match the 6–7 fold increase in sensitivity, further improvement is possible. This may be possible with the NexION 2000 because the torch base is outside the torch box and can be heated, which is not the case with the Varian 820MS.

Effect of the gap between the top of the baffle and top surface of the spray chamber. Because the 50-2 mm MC and the 75-2 mm MC enable total consumption, the gap between the upper edge of the modified baffle and the top surface of the spray chamber was changed to see if a further improvement in
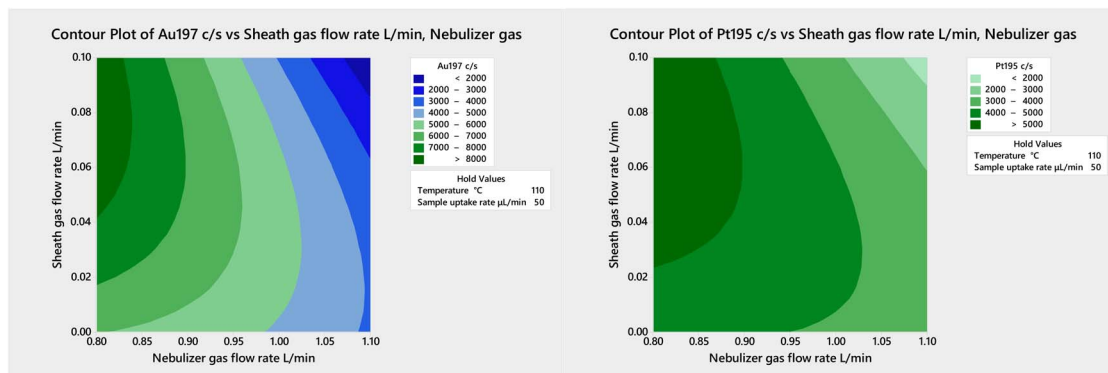
Fig. 3 Contour plots of blank-subtracted signal intensity of 5 μg L^{-1} Au (left) and Pt (right) from multivariate optimizations of sheath gas flow rate and nebulizer gas flow rate on the Varian 820MS using the 50-2 mm MC IR-heated at 110 °C and a 50 μL min^{-1} sample uptake rate.
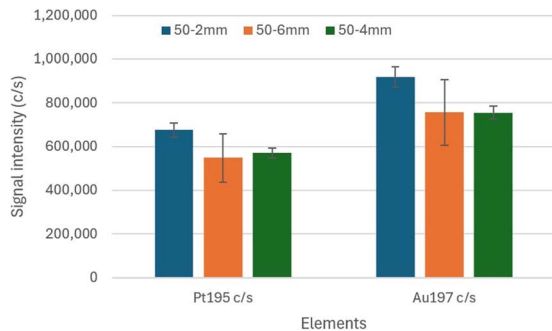
Fig. 4 Blank-subtracted signal intensity for 5 μg L^{-1} multielement solution with 110 °C IR-heated 50-2 mm, 50-4 mm and 50-6 mm MC spray chambers for Pt and Au with Varian 820MS.

performance was possible. Fig. 4 shows that sensitivity noticeably declined as the gap increased from 2 to 6 mm. According to a Student's t-test at the 95% confidence level, the signal intensity with the 50-2 mm MC is significantly higher than that with the other two chambers, and there is no significant difference between the signals obtained with the 50-4 mm MC and the 50-6 mm MC. Furthermore, according to an F test at the 95% confidence level, the variance with the 50-2 mm MC is significantly smaller than with the 50-4 mm MC. By restricting the flow of aerosol out of the spray chamber, the 2 mm gap likely increases the residence time of larger droplets in the chamber, thereby better enabling their pre-evaporation through IR heating. The gap between the baffle and the spray chamber's upper surface thus plays an important role in ensuring precise measurements. Considering sensitivity and precision, the 50-2 mm MC should provide the lowest DL of the three 50 mL spray chambers. Very similar trends resulted with the three 75 mL spray chambers (not shown). Hence, the 50-2 mm MC and 75-

2 mm MC spray chamber configurations were used for characterization of 60 nm Au NPs and 50 nm Pt NPs.

NP characterization. Examples of the size distributions obtained with the 50-2 mm and 75-2 mm MCs as well as with the standard double-pass spray chamber are shown in Fig. 5, with the average particle sizes and particle number concentrations from 5 replicate measurements summarized in Table 4. Clearly, the IR-heated sample introduction systems provided similar results as the conventional sample introduction system without any measurement of the transport efficiency, thereby eliminating an important source of error, for both 60 nm Au and 50 nm Pt NPs. It also eliminates sample waste and any bias associated with the filtering out of large droplets by the Scott double-pass spray chamber. Indeed, because the IR-heated 50-2 mm MC and 75-2 mm MC provide total consumption, they enable the detection of NPs present in the large droplets that are filtered out by the standard spray chamber, thus resulting in a broadening of the size distribution.

Implementation of IR-heated sample introduction system on another ICPMS instrument. The 25-2 mm, 50-2 mm and 75-2 mm MCs were also tested on the NexION 2000 instrument, using the optimum IR-heating temperature and sample uptake rate found with the Varian 820MS, to check if they are independent of the ICPMS instrument. Only the nebulizer gas flow rate was optimized with the standard cyclonic spray chamber and found to be 1.00 L min^{-1} for both Au and Pt. Under these conditions, the transport efficiencies with the 50-2 mm and 75-2 mm MCs (Table 5) were identical to those found with the Varian 820MS (Table 2), confirming that their performance was independent of the ICPMS instrument. In the case of the 25-2 mm MC, total consumption was also achieved, in contrast to the less than 100% transport efficiency in Table 4, which indicates that direct connection to the base of the torch eliminated
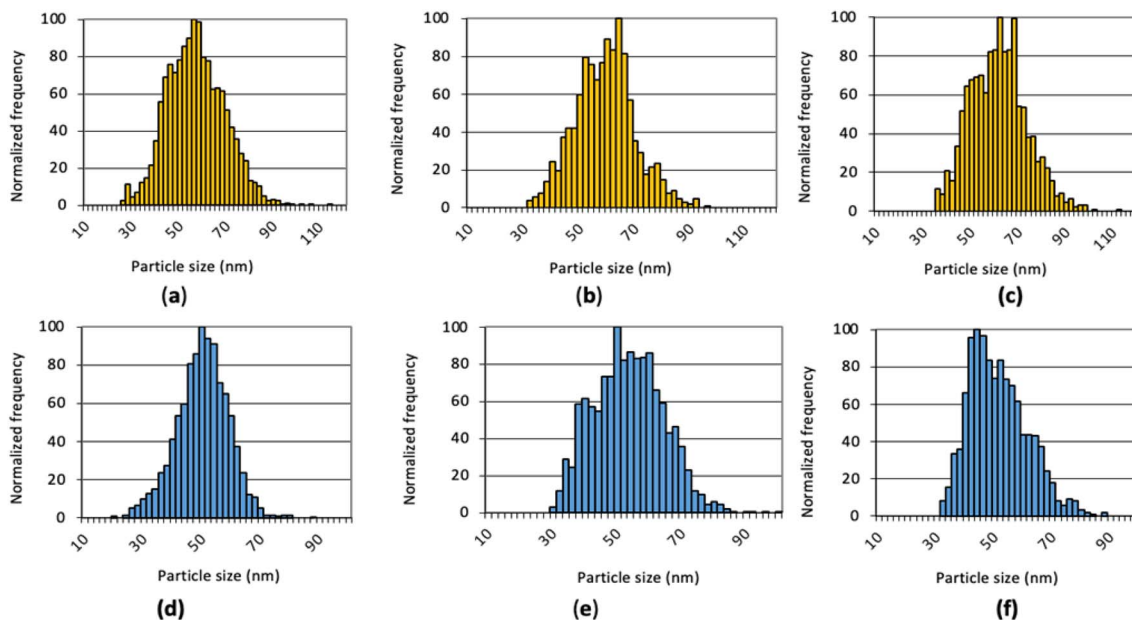

Fig. 5 Examples of normalized particle size distribution using Varian 820MS for 60 nm Au NPs (a–c) and 50 nm Pt NPs (d–f) measured by unheated Scott double-pass spray chamber (a and d); 50-2 mm MC IR-heated at 110 °C (b and e); and 75-2 mm MC IR-heated at 120 °C (c and f).

Table 4 Measured NP size (expressed as mean ± standard deviation, $n = 5000-7000$ NPs) and concentration (expressed as mean ± standard deviation, $n = 5$) for reference Au and Pt NPs with different spray chambers on Varian 820MS and NexION 2000

Instrument	Spray chamber	Mean Au NP measured size (nm)	Particle number concentration (mL^{-1})	Mean Pt NP measured size (nm)	Particle number concentration (mL^{-1})
Varian 820MS	25-2 mm MC IR-heated at 70 °C	58 ± 10	99 000 ± 11 000	49 ± 10	92 300 ± 6700
	50-2 mm MC IR-heated at 110 °C	60 ± 11	109 600 ± 7500	52 ± 11	93 400 ± 6700
	75-2 mm MC IR-heated at 120 °C	58 ± 11	94 400 ± 5800	49 ± 10	99 200 ± 5900
	Scott double-pass	55 ± 12	101 700 ± 5900	49 ± 9	99 000 ± 5000
NexION 2000	25-2 mm MC IR-heated at 70 °C	65 ± 11	92 300 ± 5500	47 ± 9	97 800 ± 9700
	50-2 mm MC IR-heated at 110 °C	69 ± 10	109 600 ± 7500	55 ± 7	102 800 ± 5700
	75-2 mm MC IR-heated at 120 °C	62 ± 19	94 500 ± 7800	59 ± 11	99 200 ± 8900
	Cyclonic	65 ± 8	95 200 ± 6900	52 ± 5	103 400 ± 5900
	Reference value	60.6 ± 5.9	100 000	50 ± 4	100 000

Table 5 Figures of merit for spICPMS with 4 different volume spray chambers under optimum conditions on NexION 2000

Spray chamber	Cyclonic	25-2 mm MC	50-2 mm MC	75-2 mm MC
IR temperature (°C)	20	70	110	120
Sample uptake rate (μL min^{-1})	600 ± 23	50.0 ± 5.0	50.0 ± 5.0	50.0 ± 5.0
Transport efficiency (%)	10.1 ± 1.8	103.9 ± 6.4	105.2 ± 6.5	94 ± 15
^{195}Pt sensitivity (counts s^{-1} μg^{-1})	4.16×10^{10}	9.49×10^{10}	1.77×10^{11}	1.32×10^{11}
^{197}Au sensitivity (counts s^{-1} μg^{-1})	6.4×10^{10}	2.01×10^{11}	3.49×10^{11}	2.00×10^{11}
^{195}Pt solution DL (ng L^{-1})	12	6.5	4.3	7
^{197}Au solution DL (ng L^{-1})	11	9.2	4.5	8
^{195}Pt method size DL (nm)	25	24	11	18
^{197}Au method size DL (nm)	28	14	10	17

the loss that could occur in the unheated region between the sheathing device and base of the torch in the torch box of the Varian 820MS when IR-heating at a sub-boiling temperature. Although the standard spray chamber is different with the NexION 2000 (cyclonic) than with the Varian 820MS (double-pass), they provided a similar sample transport efficiency when used with the same nebulizer.

Furthermore, Table 6 shows that similar improvements in sensitivity and DLs were achieved as in Table 2, irrespectively of

the ICPMS instrument. However, despite removal of the sheathing device and direct heating of the torch base when using the NexION 2000, the improvement in method DL remained lower than in sensitivity. Even the solution DL did not improve as much as sensitivity on the NexION 2000 with an IR-heated MC. This may be due to the handmade torch connector with Teflon sleeve that was used to connect the spray chamber elbow to the torch. A one-body quartz adapter will be fabricated and tested in future work to see if it improves precision. Alternatively, the

Table 6 Improvement in sensitivity and size DL with 70 °C IR-heated 25-2 mm MC, 110 °C IR-heated 50-2 mm MC and 120 °C IR-heated 75-2 mm MC for Pt and Au with Varian 820MS and NexION 2000 instruments *versus* a standard sample introduction system

Figure of merit	25-2 mm MC IR-heated at 70 °C		50-2 mm MC IR-heated at 110 °C		75-2 mm MC IR-heated at 120 °C	
	Varian 820MS	NexION 2000	Varian 820MS	NexION 2000	Varian 820MS	NexION 2000
Pt sensitivity ratio (MC/standard)	10.2	2.3	5.9	4.3	4.4	3.2
Au sensitivity ratio (MC/standard)	13.2	3.1	7.0	5.5	3.8	3.0
Pt solution DL ratio (standard/MC)	3.3	1.8	7.1	2.8	1.5	1.7
Au solution DL ratio (standard/MC)	4.8	1.2	4.2	2.4	1.4	1.4
Pt method DL ratio (standard/MC)	2.0	1.1	3.7	2.2	1.6	1.4
Au method DL ratio (standard/MC)	2.9	2.0	2.6	2.8	1.4	1.7

2084 | *J. Anal. At. Spectrom.*, 2024, **39**, 2078–2086

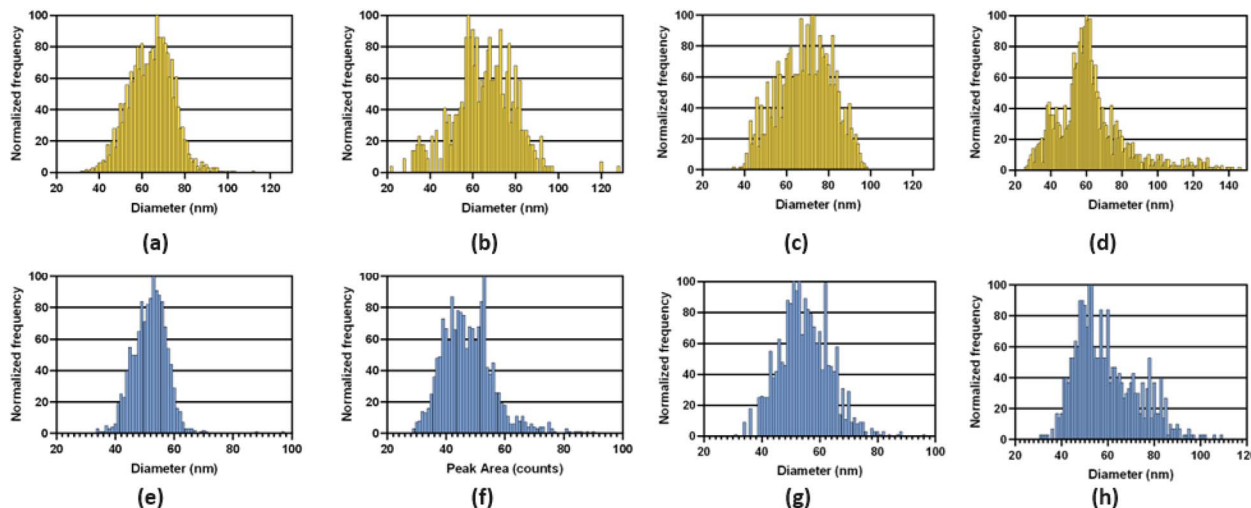This journal is © The Royal Society of Chemistry 2024

Fig. 6 Examples of normalized particle size distribution using NexION 2000 for 60 nm Au NPs (a–d) and 50 nm Pt NPs (e–h) measured by unheated cyclonic spray chamber (a and e); 25-2 mm MC IR-heated at 70 °C (b and f); 50-2 mm MC IR-heated at 110 °C (c and g); and 75-2 mm MC IR-heated at 120 °C (d and h).

outlet of the elbow connecting the spray chamber to the torch will be modified so that it connects directly to the torch.

Examples of the size distributions obtained with the three MCs providing total consumption on the NexION 2000 are compared to those with the standard cyclonic spray chamber in Fig. 6. As observed on the Varian 820MS, the size distributions with the MCs are broader than with the standard system because everything is measured. The filtration process with the cyclonic spray chamber preferentially removes large droplets and may concurrently remove larger NPs. On the other hand, large droplets containing more than one NP may result in larger NPs following IR heating, if agglomeration is induced by pre-evaporation of water. Analysis of NPs suspensions with an increasing dilution factor will reveal if larger NPs are present, as the distribution would not be affected, or if small NPs agglomerate upon pre-evaporation, if the size of larger NPs decreases upon an increase in dilution factor. In any case, accurate sizing measurements and NP concentrations were obtained with all systems, as shown in Table 4. As this performance was achieved using the operating conditions optimized with the standard sample introduction system, multivariate optimization of the sampling position, nebulizer gas flow rate, IR-heating temperature, and sample uptake rate will be carried out with each spray chamber to further improve the results and find conditions providing a good balance between sensitivity, detection limit and plasma robustness.

Conclusions

In this research, an IR-heated sample introduction system was optimized for spICPMS to achieve total sample consumption and eliminate the requirement to measure the transport efficiency. All IR-heated MC systems improved sensitivity and transport efficiency compared to those achieved with a conventional Scott double-pass spray chamber on the Varian 820MS or

cyclonic spray chamber on the NexION 2000. The 50-2 mm MC spray chamber IR-heated at 110 °C not only provided total consumption but also improved sensitivity and detection limit to a greater extent than in the previous work with the same system on the same instrument.[26] Clearly, the use of glass-fiber insulating tape effectively assisted in sustaining a consistent temperature within the connection between the spray chamber and the torch, thereby resulting in improved measurement precision by reducing background noise and enhancing transport efficiency. The system allows accurate size measurement of Au and Pt NPs without measurement of transport efficiency. Thus, IR heating the sample introduction system facilitates spICPMS analysis.

Future work will involve a more straightforward connector between the spray chamber and the base of the torch on the NexION 2000 ICPMS instrument and a more detailed optimization of the nebulization conditions with each MC chamber. To verify the increased plasma robustness provided by the fully optimized system, which introduces water in vapor form in the plasma, it will be applied to the analysis of a variety of NPs in various matrices, including environmental ones. This will include mixtures of NPs with dissolved analyte. Depending on the background signal intensity of the measured samples, different statistical approaches may be employed to determine the particle detection threshold. When dealing with low background counts, Poisson statistics are more appropriate than Gaussian statistics, as the latter may not provide a valid representation of the data distribution.[28] To ensure accurate and reliable NP detection, a comprehensive comparison between Poisson statistics and Gaussian distribution will be conducted.

Data availability

Data for this article, including multiple optimizations, figures of merit, and nanoparticle suspension characterization are

available at Open Science Framework at **https://doi.org/10.17605/OSF.IO/RP7EC**.

Author contributions

Zichao Zhou: conceptualization, investigation, data curation, formal analysis, methodology, writing – original draft and revised draft; Mirah Burgener: investigation, methodology, funding acquisition, validation; John Burgener: investigation, methodology, funding acquisition, validation; Diane Beauchemin: conceptualization, funding acquisition, methodology, resources, project administration, supervision, writing – original draft and revised draft.

Conflicts of interest

There are no conflicts to declare.

Acknowledgements

References

1 International Organization for Standardization, *Nanotechnologies Vocabulary Part 1: Core Terms*, ISO/TS, 2001.

2 A. Mohajerani, L. Burnett, J. V. Smith, H. Kurmus, J. Milas, A. Arulrajah, S. Horpibulsuk and A. A. Kadir, *Materials*, 2019, **12**, 3052.

3 K. Schmid and M. Riediker, *Environ. Sci. Technol.*, 2008, **42**, 2253–2260.

4 B. Naseer, G. Srivastava, O. S. Qadri, S. A. Faridi, R. U. Islam and K. Younis, *Nanotechnol. Rev.*, 2018, **7**, 623–641.

5 P. Biswas and C.-Y. Wu, *J. Air Waste Manage. Assoc.*, 2005, **55**, 708–746.

6 C. M. Hoo, N. Starostin, P. West and M. L. Mecartney, *J. Nanopart. Res.*, 2008, **10**, 89–96.

7 E. Tomaszewska, K. Soliwoda, K. Kadziola, B. Tkacz-Szczesna, G. Celichowski, M. Cichomski, W. Szmaja and J. Grobelny, *J. Nanomater.*, 2013, **2013**, 1–10.

8 T. G. F. Souza, V. S. T. Ciminelli and N. D. S. Mohallem, *J. Phys.: Conf. Ser.*, 2016, **733**, 012039.

9 M. D. Montaño, J. W. Olesik, A. G. Barber, K. Challis and J. F. Ranville, *Anal. Bioanal. Chem.*, 2016, **408**, 5053–5074.

10 K. Tiede, A. B. A. Boxall, S. P. Tear, J. Lewis, H. David and M. Hassellov, *Food Addit. Contam.: Part A*, 2008, **25**, 795–821.

11 M. Hassellöv, J. W. Readman, J. F. Ranville and K. Tiede, *Ecotoxicology*, 2008, **17**, 344–361.

12 R. P. Lamsal, M. S. E. Houache, A. Williams, E. Baranova, G. Jerkiewicz and D. Beauchemin, *Anal. Chim. Acta*, 2020, **1120**, 67–74.

13 C. Degueldre and P.-Y. Favarger, *Colloids Surf., A*, 2003, **217**, 137–142.

14 F. Laborda, E. Bolea and J. Jiménez-Lamana, *Anal. Chem.*, 2014, **86**, 2270–2278.

15 E. Bolea, M. S. Jimenez, J. Perez-Arantegui, J. C. Vidal, M. Bakir, K. Ben-Jeddou, A. C. Giménez, D. Ojeda, C. Trujillo and F. Laborda, *Anal. Methods*, 2021, **13**, 2742–2795.

16 D. Mozhayeva and C. Engelhard, *J. Anal. At. Spectrom.*, 2020, **35**, 1740–1783.

17 H. E. Pace, N. J. Rogers, C. Jarolimek, V. A. Coleman, C. P. Higgins and J. F. Ranville, *Anal. Chem.*, 2011, **83**, 9361–9369.

18 F.-H. Lin, S.-I. Miyashita, K. Inagaki, Y.-H. Liu and I.-H. Hsu, *J. Anal. At. Spectrom.*, 2019, **34**, 401–406.

19 F. Varenne, A. Makky, M. Gaucher-Delmas, F. Violleau and C. Vauthier, *Pharm. Res.*, 2016, **33**, 1220–1234.

20 A. Williams and D. Beauchemin, *J. Anal. At. Spectrom.*, 2022, **37**, 727–732.

21 A. Williams and D. Beauchemin, *Anal. Chem.*, 2020, **92**, 12778–12782.

22 R. Sánchez, Á. Cañabate, C. Bresson, F. Chartier, H. Isnard, S. Maestre, A. Nonell and J.-L. Todolí, *Spectrochim. Acta, Part B*, 2017, **129**, 28–36.

23 J. Kocic, D. Günther and B. Hattendorf, *J. Anal. At. Spectrom.*, 2021, **36**, 233–242.

24 S. E. Long and R. F. Browner, *Spectrochim. Acta, Part B*, 1988, **43**, 1461–1471.

25 R. Sánchez and J.-L. Todolí, *Spectrochim. Acta, Part B*, 2023, **208**, 106779.

26 Z. Zhou, A. Al Hejami, M. J. Burgener, J. Burgener and D. Beauchemin, *J. Anal. At. Spectrom.*, 2022, **37**, 1450–1454.

27 Y. Makonnen and D. Beauchemin, *Spectrochim. Acta, Part B*, 2015, **103–104**, 57–62.

28 F. Laborda, A. C. Gimenez-Ingalaturre, E. Bolea and J. R. Castillo, *Spectrochim. Acta, Part B*, 2020, **169**, 105883.

2086 | *J. Anal. At. Spectrom.*, 2024, **39**, 2078–2086

This journal is © The Royal Society of Chemistry 2024